JOURNAL OF PROPULSION AND POWER
Vol. 22, No. 4, July–August 2006

Swirler Flow Field Characteristics in a Sudden Expansion Combustor Geometry

A. Panduranga Reddy,* R. I. Sujith,† and S. R. Chakravarthy*
Indian Institute of Technology Madras, Chennai 600 036, India

DOI: 10.2514/1.15940

The present study investigates the flow field characteristics of a gas turbine swirler in a model combustion chamber, using particle image velocimetry. Detailed mean and RMS velocities, vorticity, Reynolds shear stress, and pseudoturbulent kinetic energy were obtained at various cross sections downstream of the swirler and in a plane along the inlet flow direction. The experiments were performed in a sudden expansion square geometry. A central toroidal recirculation zone and corner recirculation zone was observed and characterized. Another instability caused by swirl, called precessing vortex core, has been observed far downstream of the swirler, in the plane located at $Z/D = 2.5$ and 1.25 (D, diameter of the swirler) depending on the pressure drop across the swirler. High RMS velocity magnitudes are observed in several cross-sectional planes indicating high levels of turbulence generated by the swirling effect which promotes rapid mixing. The structure of the complex swirling flow field has been investigated both qualitatively and qualitatively.

I. Introduction

SWIRLING flows, which are highly three dimensional in nature, have the characteristics of both rotating motion and free turbulence phenomenon encountered in jets and wake flows. They occur in a wide range of applications such as gas turbines, gasoline and diesel engines, and industrial furnaces. Swirl has a large scale effect on flow fields. The simplest means of generating a swirling flow is by the use of a vane swirler to induce a tangential velocity component to an otherwise axial flow of an annular round jet [1]. If the strength of the swirl is greater than a certain critical value, the forces due to the induced pressure gradients exceed the forward kinetic forces. The flow reverses its direction on the axis of symmetry and a central toroidal recirculation zone (CTRZ) is generated.

Many researchers have worked on swirling flows issuing into a confined region. Vu and Gouldin [2] studied swirling flow surrounded by nonswirling coflow in a confined duct. Rhode et al. [3] performed static pressure probe measurements of mean velocity in a flow through a swirler suddenly expanding into a circular duct. Samimy and Langenfeld [4] and Ahmed [5] had the swirler unit located about 50 mm upstream of the sudden expansion. Al-Abdeli and Masri [6,7] used a burner with a hybrid bluff body swirl design, incorporating a central jet surrounded by a swirling annulus, to investigate turbulent isothermal swirling jets. They conclude that the precession frequency appears to be a function of swirl number as well as the Reynolds number of both the central jet and the swirling annulus. The swirling flow field in a realistically complicated geometry of a gas turbine combustor has been experimentally characterized by Bharani et al. [8]. Similar studies have also been reported in Mongia et al. [9]. The most significant finding from the bulk of these reports is that the maximum turbulent intensity ranges from ∼36% [4] to ∼100% [5], depending upon the level of swirl. This feature has also been highlighted by Mongia et al. [9].

Most of the studies mentioned above have adopted the LDV technique to determine the velocity distribution in the swirl flow field. Notable exceptions are the investigations by Kucukgokoglan and Aroussi [10] and Pruvost et al. [11], which adopt the particle image velocimetry (PIV) technique [12,13]. Kucukgokoglan and Aroussi [10] investigated the interaction of four corotating and counter-rotating isothermal swirler burner flows in a water tank. Pruvost et al. [11] performed measurements of the three mean components and turbulence intensities of the velocity field in a swirling flow, induced by a tangential inlet in an annulus. However, the data obtained from these experiments do not comprehensively characterize the recirculation zones which are predominant features of the swirling flows that determine the flame anchoring capabilities in a combustion chamber. In the recent past more experiments were carried out in this direction. Li and Gutmark [14] investigated the large scale structures in a swirl-dump combustor for both cold and combustion conditions. Gallaire et al. [15] have studied the response of a swirling jet to various azimuthal modes and frequencies forced at the nozzle exit using PIV. Various dynamical states concerned with the vortex breakdown are described as a function of swirl number.

Apart from these, the advances in the computational fluid dynamics (CFD) made it possible to predict the precessing vortex core (PVC) and the influence of side wall expansion angle and swirl generator on flow pattern using the unsteady Reynolds-averaged Navier–Stokes (U-RANS) and the k–ε model with a few limitations [16–18]. Recently many investigations [19–23] have used LES successfully for simulating the swirling flows. They point out the importance of suitable inlet boundary conditions to emulate the turbulent conditions in the laboratory experiments. They predicted several modes of precession as swirl intensity increases, in which the precession as well as the spiral structure of the flow reverses direction. They also showed that the transitions between various modes are accompanied by abrupt changes in precession frequency.

The present study investigates the flow field characteristics of a swirler in a sudden expansion model combustion chamber of square geometry, using PIV. Two-component PIV is adopted as the diagnostic technique to obtain the velocity vector field in planes along and perpendicular to the axis of the test section. The experiments were aimed at understanding the swirl flow field characteristics both qualitatively and quantitatively in a rather simple geometry which closely resembles a sector of annular combustor of a gas turbine [20]. Apart from providing exhaustive mean and turbulent velocity data, the structure and length scales of the CTRZ and CRZ obtained from the PIV measurements are also emphasized, which is not so easy to obtain with other existing techniques. The results are, quite instructive in that they indicate high levels of turbulent intensity as expected, besides allowing for examination of typical length scales of vortical structures and recirculation zone in the flow field, as mentioned earlier.

Presented as Paper 0217 at the 43rd Aerospace Sciences Meeting and Exhibit, Reno, Nevada, 10–13 January 2005; received 7 February 2005; revision received 20 November 2005; accepted for publication 22 January 2006.

*Department of Aerospace Engineering.
†Department of Aerospace Engineering; sujith@iitm.ac.in (corresponding author).

II. Experimental Procedure

The schematic of the test section and the swirler unit used in the present study are shown in Fig. 1. The test section has a square cross-section of 120 mm side, and is 500 mm long [Fig. 1a]. The exit of the test section is under ambient conditions. The test section has glass windows for optical access on all four sides; the two side faces are made entirely of glass to allow a light sheet perpendicular to the axis of the test section, whereas the top and bottom sides have a glass slit of 10 and 15 mm width, respectively, which allows light sheet along the axis of the test section. In the former arrangement, the camera is placed downstream of the exit of the test section, and in the latter, the flow field is viewed from one of the side faces. Two pressure taps, one at about 50 mm upstream of the swirler, and another on the square flange at the exit plane of the swirler, are connected to two limbs of a U-tube mercury manometer for measurement of the pressure-drop across the swirler within an uncertainty of 2.5%. The swirler is fitted to the center of a square flange of 120 mm side, which is attached to the upstream end of the test section. The swirler has an inner (hub) diameter of 33 mm and an outer diameter (D) of 40 mm, and contains 12 straight vanes inclined at an angle (ϕ) of 50° to the free stream direction as shown in Fig. 1b. The central portion of the swirler is blocked by a circular disc (hub). The experimental test facility has provision for supply of compressed air up to 6 bar from three reservoirs with a capacity of 12 m^3 each. Air enters through a settling chamber with internal dimensions of $300 \times 400 \times 300$ mm^3, into a 1.5 m long seamless tube of 50 mm internal diameter (I.D.) that leads to the swirler. The tube is fitted with 50 mm long flow straightners at its inlet. A glass tube of 50 mm I.D., 2 mm wall thickness, and 100 mm length, is fixed at the other end of the seamless tube. This glass tube section is located 100 mm upstream of the swirler, where it provides optical access for the inlet velocity measurement using PIV.

A twin resonator frequency-doubled Nd:YAG laser at 532 nm wavelength (Quantel, France, Inc., make) is used as a source of illumination for the PIV measurements in the test section. An interline transfer digital CCD camera (Pixelfly model, PCO Imaging, Germany, Inc., make) is used for acquiring the images. It has a resolution of 1360×1024 pixels. A 75 mm, F1.2 Zoom lens (Computar, Japan, Inc., make) was used for imaging the flow field of 120×120 mm. Measurements were also made in the near field of the swirler very close to the vanes covering two regions of interest (ROI) 20×20 mm and 40×40 mm named as ROI-1 and ROI-2, respectively. For this purpose still higher zoom lens with specifications 300 mm, F4.0 (DL Macro super, Sigma Japan, Inc., make) and CCD camera (SensiCam, PCO Imaging, Germany, Inc., make) with resolution 1024×1280 pixels were used. The velocities for the close-up locations were expected to be high and hence a smaller delay time between the laser pulses is required. With SensiCam, the delay between the two successive images as low as 200 ns was possible. Olive oil is used to generate tracer particles using a seeding arrangement that employs Laskin nozzles [12]. Compressed air with 0.5 to 1.5 bar pressure difference with respect to the outlet pressure is applied to the Laskin nozzles to create air bubbles of size <1 μm within the liquid. Such size of the seeding particles ensures that they follow the flow very closely [24]. The seeding particles are injected into the settling chamber to ensure proper mixing of the particles which then travel along the 1.5 m long inlet duct before entering the swirler unit. The concentration of seeding particles is controlled by fine tuning of a bypass valve. The laser and the camera are synchronized with a sequencer (SequencerV8.0 HardSoft, Germany, Inc., make). Seco2003, has been used as an interface program to generate the transistor transistor logic pulses from the sequencer in a required sequence. More than 200 pairs of instantaneous images are obtained for determining ensemble-averaged velocity vectors and the RMS velocity fluctuations.

The PIV images were analyzed using the cross-correlation software PivView [25][‡] on a PC. The PIV provides the velocity vector field (u, v) sampled on 2-D (x, y), evenly spaced grid

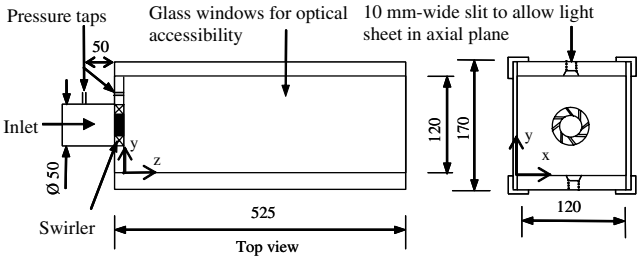

a)

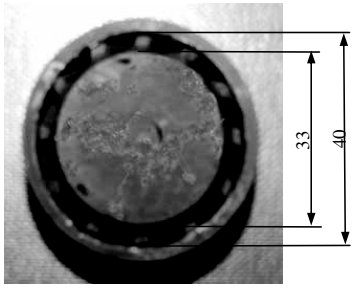

b)

Fig. 1 a) Schematic of the experimental test section with sudden expansion geometry; b) the vane swirler used in the present setup showing the hub (33 mm) and outer diameter of vanes (40 mm).

(interrogation areas). The differential quantities such as the vorticity, defined as $\omega_z = (\partial v/\partial x) - (\partial u/\partial y)$ were obtained by implementing the finite differencing scheme (least squares method) on the measured spatial velocity vector field [12]. The 2-D PIV technique is difficult to implement for a highly three-dimensional flow field such as that investigated here, because a trade-off is necessitated to obtain appreciable displacement of particles in the given time-interval between two laser pulses and to minimize out-of-plane loss of particles at the same time. The uncertainty in velocity measurement depends on several aspects extending from the recording process to the methods of evaluation as summarized in Raffel et. al. [12], pp. 134–146. The interrogation area for determining the cross-correlation of the pair of images is maintained at 64×64 pixels, with an overlap of 75% between adjacent cells in the near field of the swirler (up to $Z/D = 1.25$) and it is 32×32 pixels, with an overlap of 50% in the far field of the swirler (from $Z/D = 2.5$). The time interval between the pulses is varied in the range of 1–120 μs, depending upon the range of velocities in different regions of the flow field in different planes of the test section, so that the particle displacement obtained is ~4 pixels. A subpixel accuracy of 0.2 pixel can be obtained, which yields an uncertainty in the mean velocity measurement within ~3% [26] and for differential quantities like vorticity within 4.5%.

III. Results and Discussion

Measurements were performed for pressure drops of 0.1 and 0.05 bar across the swirler which corresponds to a Reynolds number of 32,000 and 27,000, respectively, at the inlet. A fully developed turbulent flow is established as measured in the glass tube section about $2.5D$ upstream of the swirler, with a centerline ensemble-averaged velocity of 10 and 8 m/s, respectively, under the test conditions mentioned above. The maximum value of RMS velocity as a fraction of mean velocity magnitude is observed to be around 0.09.

To characterize the swirl flow, a nondimensional number called as swirl number S, is defined as the ratio of axial flux of swirl momentum divided by the axial flux of axial momentum times the equivalent nozzle radius. The swirl number of the annular swirler with constant vane angle (α) used in the present study is given by Beer and Chigier [27]

[‡]Web address: http://www.pivtec.com [cited 25 September 2005].

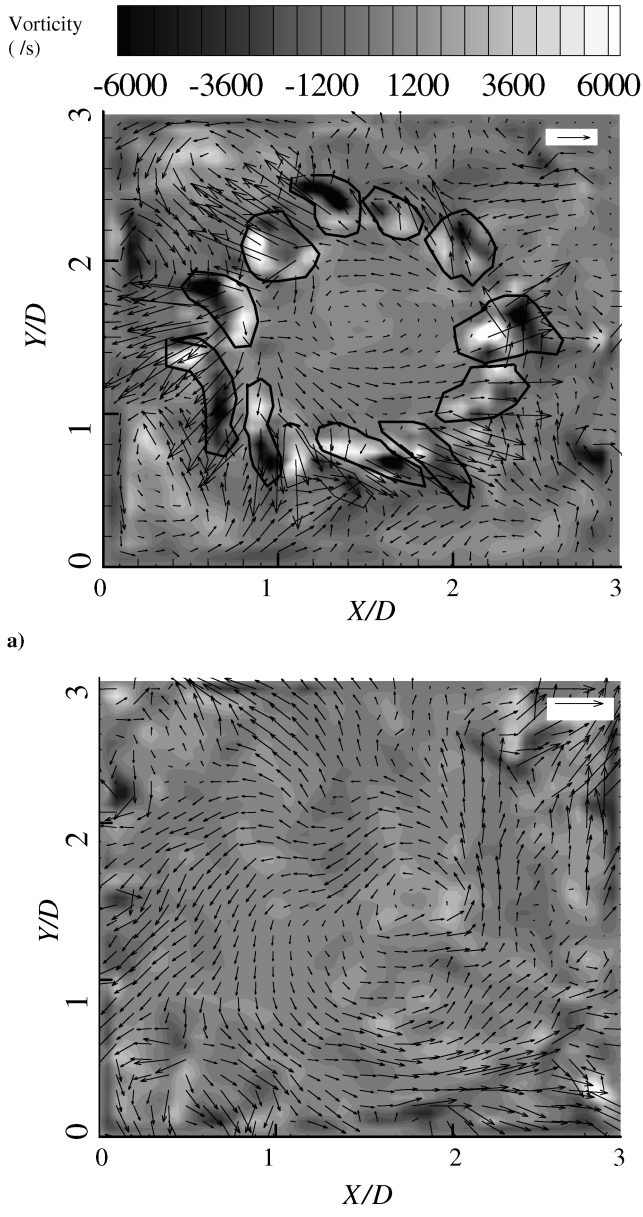

Fig. 2 The instantaneous velocity and vorticity contour plots illustrating a) vorticity pairs corresponding to each swirler vanes in the near field at plane $Z/D = 0.5$ and b) absence of vorticity pairs in plane $Z/D = 1.25$ further downstream of the swirler for pressure drop of 0.1 bar test condition. The reference vector of 15 m/s is shown at the top right corner of corresponding planes. The vectors shown are undersampled by a factor 2 in both x and y direction for clarity.

$$S = \frac{2}{3}\left[\frac{1-(D_h/D)^3}{1-(D_h/D)^2}\right]\tan\alpha$$

where D_h = diameter of the hub (33 mm), D = outer diameter of the vanes (40 mm), and α is the vane angle (50 deg). Thus the swirl number is calculated to be 1.09 in the present case, which corresponds to a strong swirl .

A. 0.1 Bar Pressure Drop Test Condition

The instantaneous flow field measurements (Fig. 2) for the pressure drop of 0.1 bar show the complexity of the three dimensional swirling flow investigated in the present study. The contours of vorticity are superposed over the velocity vector fields for a better understanding of the interaction of these fields with each other. The instantaneous velocity fields in the cross-sectional plane located at $Z/D = 0.5$ from the swirler exit [Fig. 2a] shows several small-scale vortical structures distributed concentrically over the cross section of the test section. It can be observed that these vortices of high strength are paired as positive (white) and negative (black) patches alternatively corresponding to each vane in the near field of the swirler.

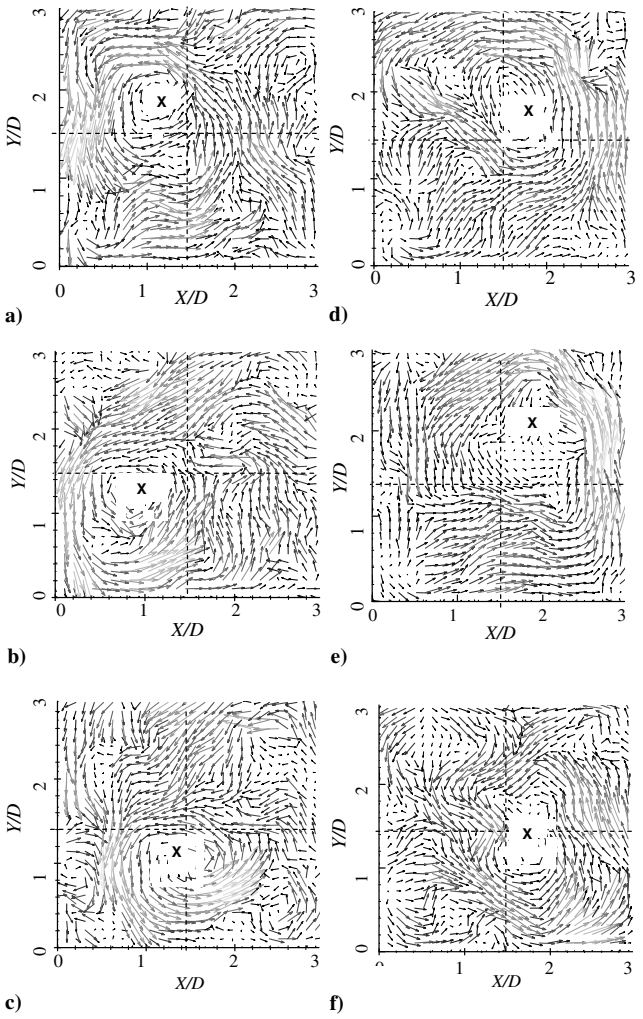

Fig. 3 PVC observed from the various instantaneous velocity vector plots a)–f) obtained in cross-sectional plane at axial location $Z/D = 2.5$, for the pressure drop of 0.1 bar test condition. The vectors shown are undersampled by a factor 2 in both x and y direction for clarity.

The flow undergoes separation at the leading and trailing edges of the swirler vanes, and also behaves as multiple jets issuing out of the individual vane passages at the exit of swirler. These features result in the effect of counter-rotating vorticity pairs that are observed to be equal in number to that of the vane passages. The typical length scales of the turbulence involved could be approximated with the swirler vane gap, that is, around 3 to 5 mm. These jets try to expand interacting with each other. High velocity gradients are observed in this region of expansion. However, proceeding a little further downstream of the swirler in plane $Z/D = 1.25$ [Fig. 2b], the strength of these pairs is observed to be declining rapidly as the flow expands into the test section and it appears to be distributed uniformly throughout the plane.

The PVC can be observed from various instantaneous velocity vector plots obtained at the cross-sectional plane located at an axial distance of $Z/D = 2.5$ downstream of the swirler as shown in Fig. 3, for the pressure drop of 0.1 bar test condition. The large cross bars represent the geometric center of the test section. The small cross "×" represent the approximate center of the precessing swirl. The swirling flow appears to be centered at a particular location, and it

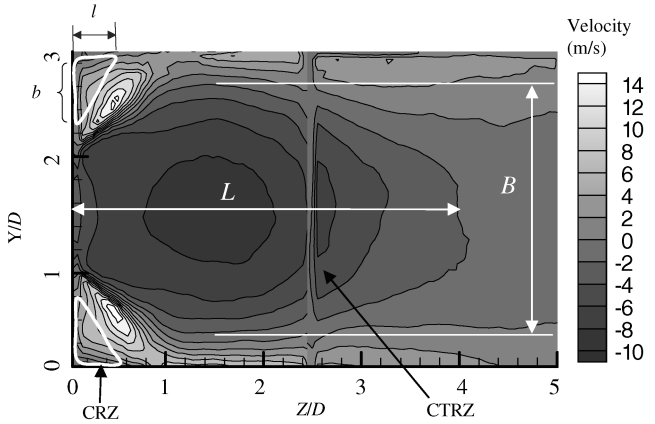

Fig. 4 The structures of the CTRZ and CRZ obtained from ensemble-averaged axial isovelocity contour plot for the pressure drop of 0.1 bar test condition.

keeps changing its position instantaneously. The center of the swirl indicated with "×" keeps precessing above the geometric axis of symmetry in counter clockwise direction [Fig. 3a–3f]. The magnitude of the velocities in this plane were observed to be varying from 5 m/s to a maximum of 18 m/s as indicated with the reference vector of 10 m/s. The existence of the PVC indicates the instability due to swirl. Spectral analysis was not performed as time series data could not be obtained at the low framing rates (2 image pairs per second), and hence the frequency of the PVC could not be determined. Thus, the results on PVC presented here are qualitative, as they were obtained from observation of several instantaneous velocity vector fields in different cross-sectional planes. The PVC appears to be persisting for a long distance downstream, at $Z/D = 2.5$, more than what is normally reported, presumably due to the confinement. These types of flow fields can be substantially affected by the exhaust configuration, the diameter, location (i.e., centrally located, off center, etc.), even when it is a long way downstream. In the present study, the exhaust was simply let to atmosphere without any extension duct.

The structure of the central toroidal recirculation zone (CTRZ) and the corner recirculation zone (CRZ) obtained for the pressure drop of 0.1 bar test condition is illustrated in Fig. 4. Over 200 velocity vector fields were ensemble averaged, and the structure of the CTRZ and CRZ was obtained from the contour of the axial velocity in the plane perpendicular to the swirler. The lengths (L, l) and widths (B, b) as shown in the figure characterize the CTRZ and CRZ, respectively. The central plane is chosen due to its easy optical accessibility compared with any other planes. It can be noted that the shape of the CRZ is considerably distorted in the circumferential direction according to the expanding geometry. For instance, on a 45° plane the CRZ width and length would be expected to be larger compared with the central plane whereas as the CTRZ width and the length will remain same, as analyzed from the PIV data obtained in the cross sections, close to the swirler exit ($Z/D < 2$). The length scales of the CTRZ and CRZ observed from the plots for both the test conditions are summarized in Table 1. The values in the table are obtained by close observation of the plots with an uncertainty of 5%.

The ensemble-averaged velocity vector field, corresponding to the cross-sectional planes at $Z/D = 0.5, 0.75, 1, 1.25, 2.5$ downstream of the swirler are plotted together in a 3-D cascaded view as shown in Fig. 5a. A strong outward radially expanding swirl flow can be observed in the plane at $Z/D = 0.5$. The velocities in this plane were observed to be having a maximum value of 27 m/s. The central low

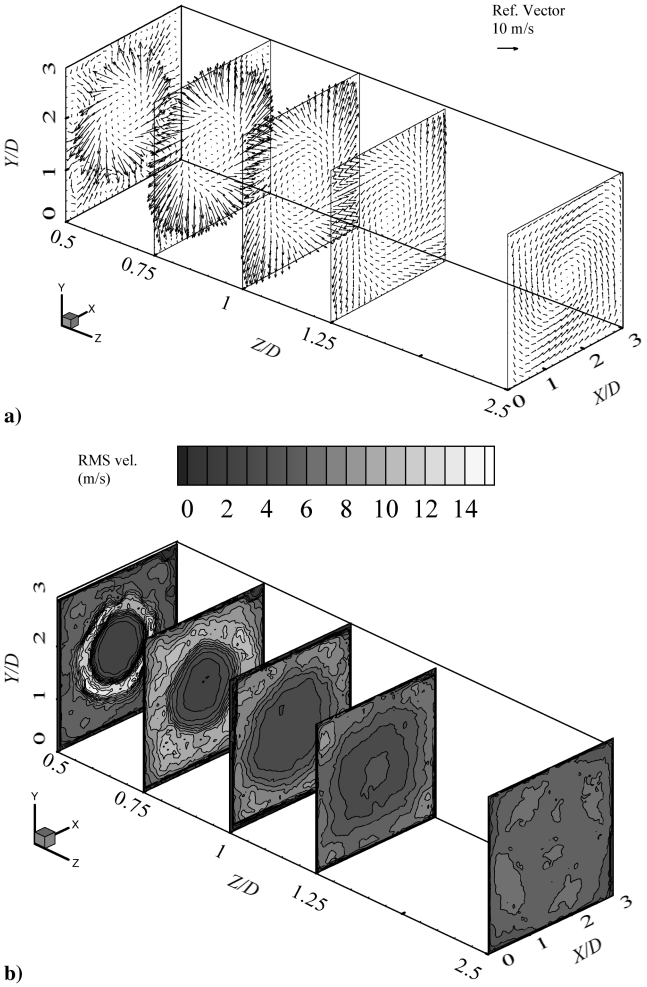

Fig. 5 a) Mean velocity vector plots (the vectors shown are undersampled by a factor 3 in both x and y direction for clarity) and b) RMS velocity magnitude ($\sqrt{\bar{u}'^2 + \bar{v}'^2}$) plots with isocontour lines in several cross-sectional planes downstream of the swirler exit for ΔP of 0.1 bar across the swirler.

velocity region (CTRZ) can be observed in this plane. Large velocity gradients are obtained in the region of interaction of CTRZ and CRZ with the jet issuing from the swirler. Subsequent near-field locations, such as at $Z/D = 0.75, 1, 1.25$ exhibit homogenization of the swirl flow field in the azimuthal direction. Proceeding further downstream of the swirler at $Z/D = 2.5, 5, 10$ (only up to $Z/D = 2.5$ is shown in the figure) the magnitude of velocities were observed to be drastically reduced. Most of the flow is observed near to the walls and velocity magnitude is approximately constant over a large area.

The turbulent velocity fluctuations are obtained from the instantaneous velocity flow field. The RMS velocity magnitude ($\sqrt{\bar{u}'^2 + \bar{v}'^2}$, where u and v in their usual notation) plots with isocontour lines obtained at several cross-sectional planes for these test condition are shown in Fig. 5b. These plots illustrate the complexity of the flow field due to high turbulence generated by the swirler. The maximum RMS velocity magnitude is measured to be around 15 m/s in the plane at $Z/D = 0.5$, where the maximum mean velocity is 27 m/s. The turbulence levels in the recirculation zones are observed to be high even where the mean flow field velocities are low, especially in the central recirculation zone along the axis of the

Table 1 The approximate length scales of the CTRZ and CRZ obtained in the meridional plane for the two pressure-drop test conditions

Pressure drop across the swirler [bar]	Length of the CTRZ [L]	Width of the CTRZ [B]	Length of the CRZ (reattachment point) [l]	Width of the CRZ [b]
0.1	4D	2.25D	0.75D	0.5D
0.05	3D	1.87D	0.5D	0.35D

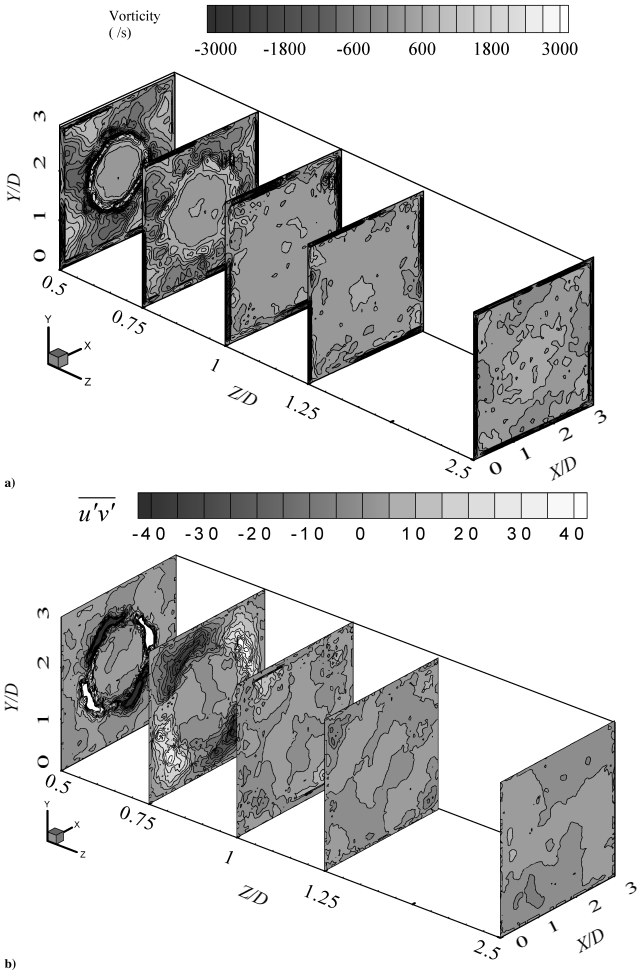

Fig. 6 a) Mean vorticity contour plots and b) Reynolds shear stress ($\overline{u'v'}$) contour plots with isocontour lines in various cross-sectional planes downstream of the swirler exit for ΔP of 0.1 bar across the swirler.

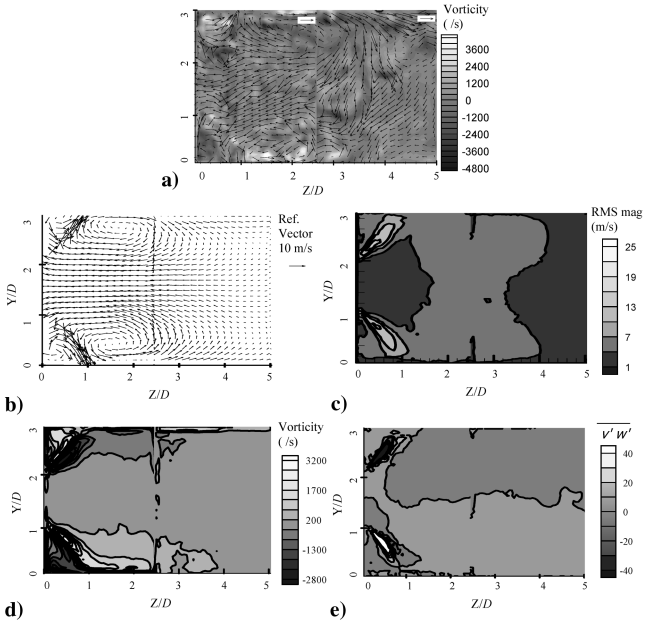

Fig. 7 a) Instantaneous vorticity overlapped with velocity vector plot; b) the mean velocity vector plot (the vectors shown are undersampled by a factor 3 in z direction and 2 in y direction for clarity); c) RMS velocity contour; d) mean vorticity contour; e) Reynolds shear stress contour, showing isocontour lines in plane along the inlet flow direction for ΔP of 0.1 bar across the swirler.

test section. The turbulence level is observed to be decaying rapidly as we proceed further downstream of the swirler. The turbulence levels are observed to be very high near the swirler essentially due to two competing effects, that is, the turbulence generated due to the flow exiting from the swirler and the flow from the CRZ and CTRZ. This substantial level of turbulence cannot be ignored in numerical models based on the Reynolds-averaging approach (RANS), which inherently assumes small levels of turbulence intensity (TI) .

The mean vorticity with isocontour lines obtained in various cross-sectional planes are shown in Fig. 6a. The instantaneous vorticity at each grid point (x, y) is ensemble averaged over several instantaneous vorticity data, that is, $\bar{w}_z(x, y) = [\sum_{i=1}^{N} w_{z,i}(x, y)]/N$ where N is the number of instantaneous values (200 PIV images) over which the ensemble average is carried out. The number of images to calculate the mean quantities was determined by means of a convergence test [27]. Two hundred images were observed to be enough to determine the ensemble average of a fluctuating quantity as $\sqrt{\bar{u}'^2}$ and $\sqrt{\bar{v}'^2}$, unlike only 100 images that were required for the mean quantities such as $\bar{u}$ etc. to converge within 3% accuracy. The mean vorticity convergence test carried out on a fixed point at $Z/D = 1.25$, and $(x, y) = (26.888, 26.88)$ indicated that even for differential quantities like vorticity measured in our case, has started to converge for 150 images within 4.5% accuracy. The vortex pairs of high strength (6000 s^{-1}) that were observed in the instantaneous images are averaged out and two circular bands of positive and negative vorticity are observed to be distributed concentrically. The Reynolds shear stress ($\overline{u'v'}$) contour plots with isocontour lines obtained in various cross-sectional planes downstream of the swirler are presented in Fig. 6b. The convergence test results indicated that $\overline{u'v'}$ and $\overline{v'w'}$ ensemble averaged over 200 images has converged within 7.5% accuracy. A thick region of high Reynolds shear stress is formed in between the two shear layers produced due to the interaction of CRZ and CTRZ with the swirling jet. This region has a high momentum exchange between the low velocity CTRZ and the high velocity swirling jet issuing from the swirler. This is an important characteristic of the swirling flow field. The magnitudes of shear stress obtained in the planes at $Z/D = 0.75$, 1, 1.25 indicate a drastic decay due to the expansion of these regions throughout the cross-sectional plane.

To measure the third velocity component (in the axial direction w), PIV measurements were made in the central plane along the test section. The laser light sheet is passed through the slits provided along the test section. The measurements were performed for a total length of $10D$ in steps of $2.5D$ each starting from the swirler exit. The results of first two locations (up to $5D$) are plotted together in a single plane (Fig. 7), for qualitative understanding of the flow features. The scales of the mean velocity, vorticity, and shear stresses contours are maintained the same as that of the cross-sectional planes for the ease of comparison. Figure 7a shows the instantaneous vorticity overlapped with the velocity vector plot. Two reference vectors (10 m/s) are used because two different regions ($Z/D = 0$ to 2.5, and 2.5 to 5) are plotted together. Also, it should be noted that these two regions were imaged at different instants. The complexity of the swirl flow field in the near field can be observed in this plot. Figures 7b–7e show the mean velocity magnitude, RMS velocity magnitude, vorticity, Reynolds shear stress contour plots including isocontour lines, obtained in this plane for the 0.1 bar pressure-drop test condition. A large recirculation bubble (CTRZ) is set up downstream of the reattachment point, in view of the flow reversal along the centerline [Fig. 7b]. A maximum of 20 m/s is observed in this plane. The velocities in the central core region are observed to be insignificant. A gradual decay of velocity magnitude is observed in the axial direction as flow straightens up at the exit of the test section. The RMS velocity fluctuations in the CTRZ is around 7 m/s at axial location $Z/D = 4$ [Fig. 7c]. It can be clearly seen that the maximum fluctuation levels are observed in the region that separates the CRZ and CTRZ. The small-scale vortices that are generated near the vanes of the swirler are now observed in the thick averaged region in the form of two separate bands [Fig. 7d]. These zones are paired as positive and negative vorticity depending upon their roll-up

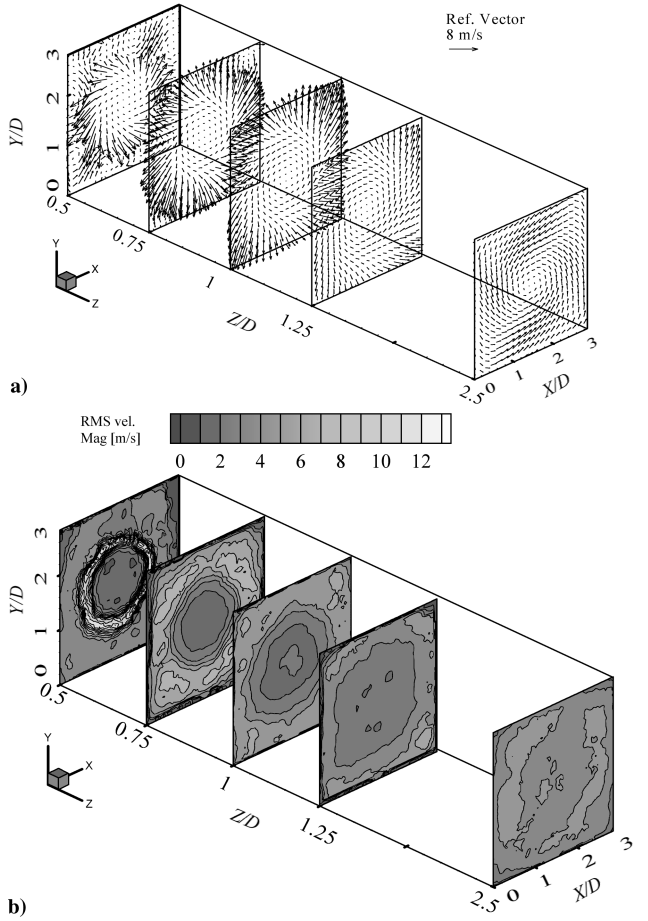

Fig. 8 a) Mean velocity vector plots (the vectors shown are undersampled by a factor 3 in both x and y direction for clarity); b) RMS velocity magnitude ($\sqrt{\bar{u}'^2 + \bar{v}'^2}$) contour plots in cross-sectional planes at different axial locations from the swirler exit for Δ P of 0.05 bar across the swirler.

direction. The magnitude of the vorticity is observed to be strong in the near field of the swirler up to $Z/D = 3$. The levels of vorticity are observed to be weak or insignificant after $Z/D = 4$, far downstream of the swirler exit. The magnitude of Reynolds stress is observed to be high in the region between the CRZ and CTRZ [Fig. 7e]. Two shear layers are observed due to interaction of the CTRZ and CRZ with the swirling jet. The decay of these stresses in a streamwise direction is very rapid, which indicates a significant diffusion and dissipation of the turbulence in the streamwise direction.

B. 0.05 Bar Pressure Drop Test Condition

This section discusses a few results obtained for the 0.05 bar pressure drop across the swirler test condition. This corresponds to an inlet velocity of 8 m/s ($Re = 27,000$) measured inside the glass tube. The mean velocity vector field corresponding to the cross-sectional planes at $Z/D = 0.5, 0.75, 1, 1.25, 2.5$ downstream of the swirler are plotted together in a 3-D cascaded view as shown in Fig. 8a. A strong outward radially expanding swirl flow can be observed in the plane at $Z/D = 0.5$. The maximum velocity in this plane was observed to be 17 m/s. Subsequent near-field locations, such as at $Z/D = 0.75, 1, 1.25$ exhibit homogenization of the swirl flow field in the tangential direction. The reattachment of the swirling jet with the walls of the test section is observed at $Z/D = 0.75$ plane, which was observed at $Z/D = 1$ for the 0.1 bar test condition.

The RMS velocity magnitude plots obtained at several cross-sectional planes for these test condition are shown in Fig. 8b. The fluid elements at the boundary of the recirculation zones have an equal probability to move in all the directions. Therefore, due to high fluctuations in the flow field, the mean velocity magnitude is very less

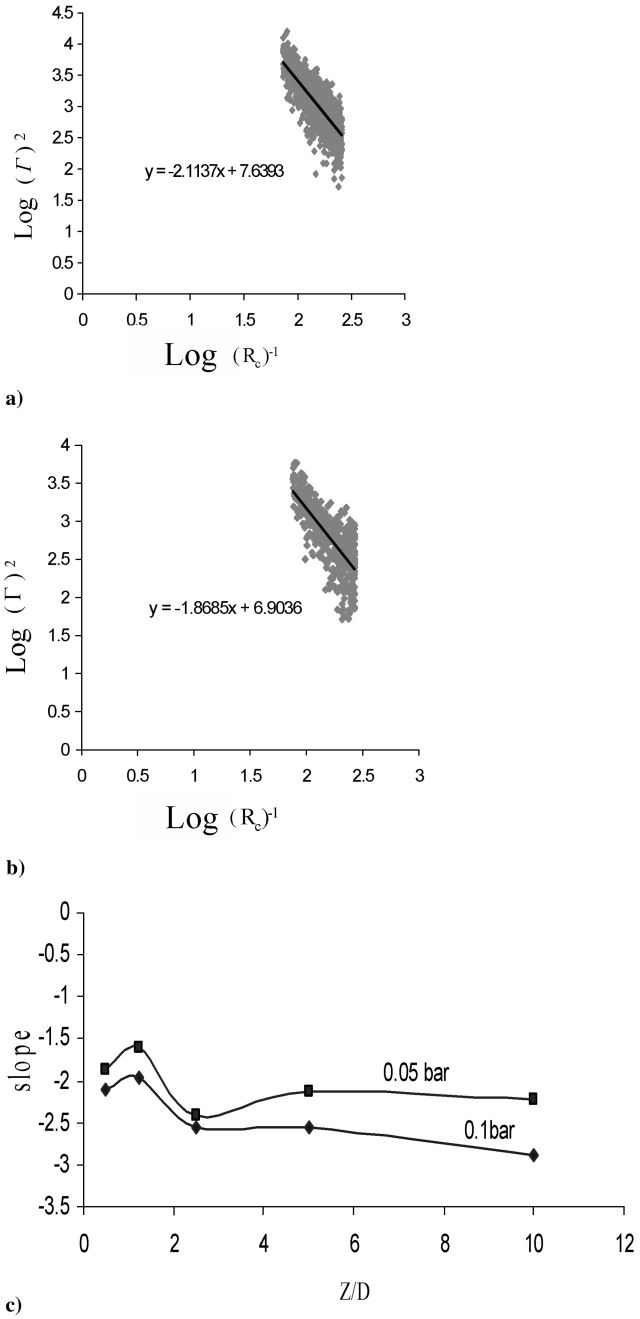

Fig. 9 Pseudoturbulence energy spectrum calculated on the basis of the vortex core diameters and squared circulations of the detected vortices at $Z/D = 0.05$ for a) 0.1 bar and b) 0.5 bar pressure-drop test conditions. The straight lines in plots a) and b) represent the slope of the turbulence energy spectrum. c) The variation in slope of several cross-sectional planes downstream of the swirler for both the test conditions.

in these regions. Hence in the $Z/D = 0.5$ plane, the regions with high turbulence levels are observed in the corners as well as in the central core region. At $Z/D = 0.75$ plane there is a decrease in turbulence level from the corners of the test section whereas, a slight increase is observed in the central recirculation zone.

C. Pseudoturbulence Energy Spectrum

Pseudoturbulence energy spectrum has been calculated on the basis of vortex core diameters and squared circulations of the detected vortices [28]. A coherent structure detection algorithm, based on the properties of selectivity in space and scale of the continuous wavelet transform was used for this purpose. The vortex core radii and circulation are determined using wavelet analysis of

PIV data. The wavelet used is the two dimensional isotropic Marr (Mexican hat) wavelet (ψ) given by

$$\psi(r,l) = \frac{1}{r}\left[2 - \left(\frac{r}{l}\right)^2\right]\exp\left(-\frac{r^2}{2l^2}\right)$$

The square of circulation versus the inverse of core size associated with the detected eddy structures corresponding to $Z/D = 0.5$ for the pressure drop of 0.1 and 0.05 bar test condition are illustrated in Figs. 9a and 9b, respectively. This illustration is different in several aspects than the classical power spectrum obtained using fast Fourier transform where the energy versus wavelength of a sine and cosine base (wave number) is presented. In an isotropic and homogeneous turbulence [29] this spectrum may contain an inertial regime with a decaying slope of $-5/3$. In the present study, the slopes of the average results using the ensemble of the detected vortices corresponding to each cross-sectional area were investigated. These slopes were observed to be converging within 2% accuracy and were varying from -1.49 to -2.9 depending upon their location [Fig. 9c]. The shaded region is approximated with a least square fit. The straight line thus obtained represents the slope of the energy spectrum decay. A slope of -3 was observed by Schram [30] for his experiments on flow over a backward facing step.

The pseudoturbulence energy spectrum obtained on the basis of vortex core diameters and squared circulations of the detected vortices in several cross-sectional planes gives an insight of the turbulence energy spectrum from the measured PIV data in this flow field. Further work would be needed to investigate the relationship between the instantaneous scales characterizing the eddy structures and the wavelengths at a given location from a FFT based energy spectrum that is usually used to characterize turbulent flows.

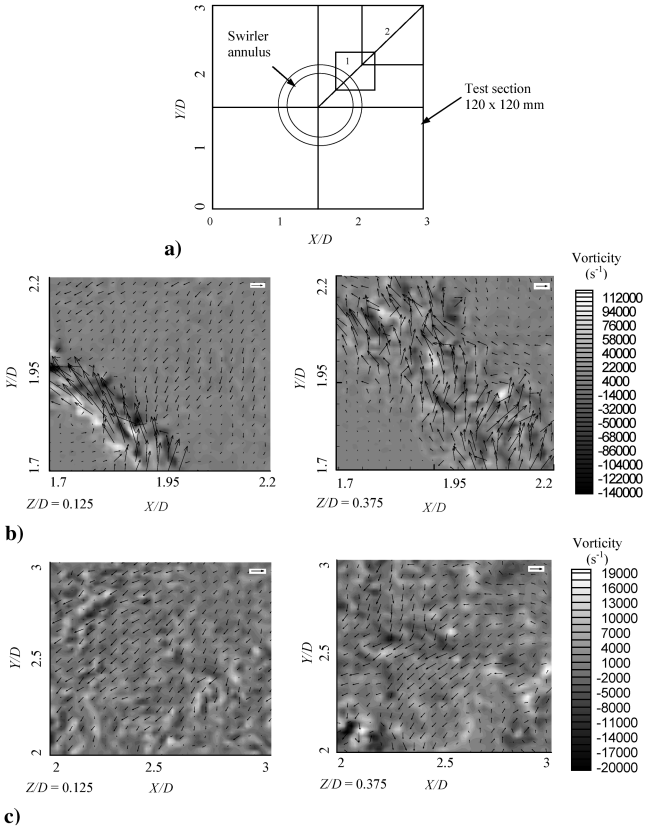

Fig. 10 a) Schematic representation of the ROI-1 and ROI-2 investigated; b) and c) instantaneous velocity vector and vorticity contour plots obtained for ROI-1 and ROI-2 (respectively) in two different planes downstream of the swirler. Reference vector: 20 m/s. The vectors shown are undersampled by a factor 3 in both *x* and *y* direction for clarity.

D. Close-Up Locations

As mentioned earlier, experiments were also performed in very near field of the Swirler ($Z/D = 0.125$, 0.25, and 0.375), covering two regions of interest of 20×20 mm (ROI-1) and 40×40 mm (ROI-2). These two locations are chosen such that they provide details of the flow field in one full quadrant of the test section as shown in Fig. 10a. The instantaneous velocity vector plot superposed by vorticity contour at $Z/D = 0.125$, 0.375 are shown in Figs. 10b and 10c for the ROI-1 and ROI-2, respectively. The vorticity magnitude is observed to be varying from $-140,000$ to $112,000$ s^{-1} and the velocity magnitudes are varying from 2 to 90 m/s in the ROI-1. The air passing through the vane passages expands suddenly into the test section producing sharp velocity gradients in the radial direction. This creates a high level of shear at the jet boundary, which is the cause for large vorticity magnitudes near the tip of the vanes. It can be observed from ROI-2 that the flow through the corner is entrained into the jet, which describes clearly the corner effects in sudden expansion geometry as investigated in the present study.

The overall flow field structure near to a single swirler vane was observed from the mean velocity vector field in ROI-1 (not shown in the interest of space). The magnitudes of mean velocity and vorticity are observed to be reducing drastically as the flow expands into the test section. The mean velocity flow field obtained at ROI-2, gives the structure of the CRZ. This corner recirculation zone acts as a secondary flame stabilization ring around the central recirculation zone. The RMS velocity magnitude contour plots (Fig. 11) show high levels of turbulence. The mixing of the corner and central recirculated air with the swirling jet issuing from the vane slots due to

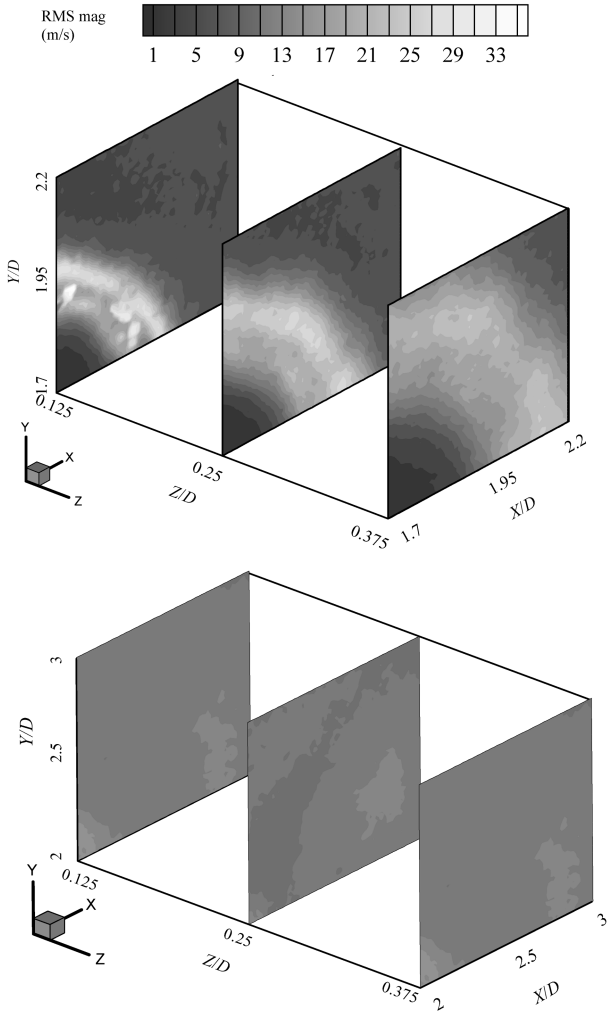

Fig. 11 RMS velocity magnitude contour plots obtained in a) ROI-1 and b) ROI-2 for various cross-sectional planes downstream of the swirler for pressure drop of 0.1 bar test condition.

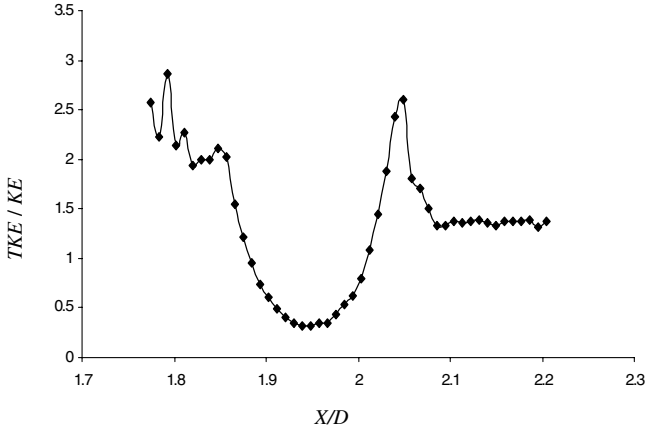

Fig. 12 Turbulent kinetic energy normalized with mean kinetic energy ($[\bar{u}'^2 + \bar{v}'^2 + \bar{w}'^2]/[\bar{u}^2 + \bar{v}^2 + \bar{w}^2]$), obtained along a line in plane at $Z/D = 0.125$ downstream of the swirler.

high turbulence can be illustrated from Fig. 11a. Comparatively low levels of RMS velocity magnitude are observed in the ROI-2 [Fig. 11b]. As observed from the figure, the low velocity recirculated fluid in the corner gains the turbulence energy as the fluid starts to entrain into the jet issuing from the vanes. Thus the RMS velocity magnitude in the CRZ increases as the flow expands into the test section until the reattachment point.

Turbulent kinetic energy (TKE) is obtained along a line (from $X/D = 1.7$ to 2.2) using the PIV data from the plane perpendicular to the swirler and the cross-sectional plane at $Z/D = 0.125$. The TKE is normalized with the mean kinetic energy ($[\bar{u}'^2 + \bar{v}'^2 + \bar{w}'^2]/[\bar{u}^2 + \bar{v}^2 + \bar{w}^2]$) is shown in Fig. 12. A maximum value of normalized TKE as high as three is observed on the inner and outer edges of the annular jet, due to formation of the shear layer by CRZ and CTRZ, respectively. The TKE attains a minimum value within the jet, exiting from the vane passage.

IV. Conclusions

This paper presents the experimental investigation performed to measure the mean and turbulent velocity fluctuations of a 3D swirling flow in a sudden expansion square geometry using PIV. The measurements have been performed for the pressure drops of 0.1 and 0.05 bar across the swirler which corresponds to a Reynolds number of 32,000 and 27,000, respectively, at the inlet to the swirler. The swirling flow features such as corner recirculation zone (CRZ), precessing vortex core (PVC), and central toroidal recirculation zone (CTRZ) were observed and characterized. The magnitudes of the velocities inside the CTRZ are low. As the pressure drop across the swirler was varied from 0.1 to 0.05, the length of the CTRZ has been decreased from 4D to 3D and width from 2.25D to 1.87D. The turbulence levels are observed to be very high in the near field of the swirler essentially due to two competing effects; that is, the turbulence generated due to the flow exiting from the swirler and the flow from the CRZ and CTRZ. The PVC effect appears to be persisting for a long distance downstream, at $Z/D = 2.5$, more than normally reported values, presumably due to the confinement. The experiments performed in the very near field of the swirler ($Z/D = 0.125, 0.25$, and 0.375), also indicates the complexity of the swirl flow field in a sudden expansion geometry both qualitatively and quantitatively.

RMS velocity and the vorticity contour plots obtained in several cross-sectional planes illustrate the complexity of the swirl flow field. The RMS velocity magnitude is observed to be as high as 15 m/s, indicating the significant level of the turbulent velocity fluctuations over the mean velocity (up to 27 m/s) flow field for pressure drop of 0.1 bar test condition. Pseudoturbulence energy spectrum plots have been obtained on the basis of vortex core diameters and squared circulations of the detected vortices. These plots show a negative slope varying from 1.49 to 2.9 and 1.6 to 2.4 for 0.1 and 0.05 bar pressure-drop test conditions, respectively. Further work would be needed to investigate the relationship between the instantaneous scales characterizing the eddy structures and the wavelengths at a given location from a FFT based energy spectrum that is usually used to characterize turbulent flows.

This set of results can also be used to anchor CFD calculations based on relatively simplistic Reynolds-averaged Navier–Stokes or large eddy simulation.

Acknowledgements

The authors wish to acknowledge the support of the Gas Turbine Research Establishment (GTRE), Bangalore, India. The interest taken by Venkataraman Shankar and Sampath Kumaran from GTRE in this work is greatly appreciated.

References

[1] Gupta, A. K., Lilley, D. G., and Syred, N., *Swirl Flows, Energy and Engineering Science Series*, Abacus Press, London, U.K., 1984.

[2] Vu, B. T., and Gouldin, F. C., "Flow Measurements in a Model Swirl Combustor," *AIAA Journal*, Vol. 20, No. 5, 1982, pp. 642–651.

[3] Rhode, D. L., Lilley, D. G., and McLaughlin, D. K., "Mean Flow Fields in Axisymmetric Combustor Geometries With Swirl," *AIAA Journal*, Vol. 21, No. 4, 1983, pp. 593–600.

[4] Samimy, M., and Langenfeld, C. A., "Experimental Study of Isothermal Swirling Flows in a Dump Combustor," *AIAA Journal*, Vol. 26, No. 12, 1988, pp. 1442–1449.

[5] Ahmed, S. A., "Velocity Measurements and Turbulence Statistics of a Confined Isothermal Swirling Flow," *Experimental Thermal and Fluid Science*, Vol. 17, No. 3, 1998, pp. 256–264.

[6] Al-Abdeli, Y. M., and Masri, A. R., "Precession and Recirculation in Turbulent Swirling Isothermal Jets," *Combustion Science and Technology*, Vol. 176, No. 5–6, 2004 pp. 645–665.

[7] Al-Abdeli, Y. M., and Masri, A. R., "Recirculation and Flow Field Regimes of Unconfined Non-Reacting Swirling Flows," *Experimental Thermal and Fluid Science*, Vol. 27, No. 5, 2003, pp. 655–665.

[8] Bharani, S., Singh, S. N., and Agrawal, D. P., "Effect of Swirl on the Flow Characteristics in the Outer Annulus of a Prototype Reverse-Flow Gas Turbine Combustor," *Experimental Thermal and Fluid Science*, Vol. 25, No. 6, June 2001, pp. 337–347.

[9] Mongia, H. C., Gore, J. P., Grinstein, F. F., Gutmark, E. J., Jengand, S. M., McDonell, V. G., Menon, S., Samuelson, G. S., and Santoro, R. J., "Combustion Research Needs for Helping Development of Next-Generation Advanced Combustors," *37th AIAA/ASME/SAE/ASEE Joint Propulsion Conference & Exhibit*, AIAA Paper 2001-3853, July 2001.

[10] Kucukgokoglan, S., and Aroussi, A., "Isothermal Swirling Burner Flow Measurements," *Proceedings of the 4th International Symposium on Particle Image Velocimetry*, Paper 1074, Sept. 2001.

[11] Pruvost, J., Legrand, J., and Doubliez, L., "Particle Image Velocimetry Investigation of the Flow-Field of a 3D Turbulent Annular Swirling Decaying Flow Induced by Means of a Tangential Inlet," *Experiments in Fluids*, Vol. 29, 2000, pp. 291–301.

[12] Raffel, M., Willert, C. E., and Kompenhans, J., *Particle Image Velocimetry, A Practical Guide*, Springler–Verlag, New York, 1998, Chaps. 2, 4, 5, and 6.

[13] Westerweel, J., Draad, A. A., Th, J. G., Van der Hoeven, and Van Oord, J., "Measurement of Fully-Developed Turbulent Pipe Flow with Digital Particle Velocimetry," *Experiments in Fluids*, Vol. 20, No. 3, 1996, pp. 165–177.

[14] Li, G., and Gutmark, E. J., "Experimental Study of Large Coherent Structures in a Swirl—Dump Combustor," *42nd AIAA Science Meeting and Exhibit.*, Jan. 2004

[15] Gallaire, F., Rott, S., and Chomaz, J. M., "Experimental Study of a Free Swirling Jet," *Physics of Fluids*, Vol. 16, No. 8, 2004, pp. 2907–2917.

[16] German, A. E., and Mahmud, T., "Modelling of Non-Premixed Swirl Burner Flows Using a Reynolds-Stress Turbulence Closure," *Fuel*, Vol. 84, No. 5, 2005, pp. 583–594.

[17] Yang, S. L., Siow, Y. K., Peschke, B. D., and Tacina, R. R., "Numerical Study of Nonreacting Gas Turbine Combustor Swirl Flow Using Reynolds Stress Model," *Journal of Engineering for Gas Turbines and Power*, Vol. 125, No. 3, July 2003, pp. 804–811.

[18] Mondal, S., Datta, A., and Sarkar, A., "Influence of Side Wall Expansion Angle and Swirl Generator on Flow Pattern in a Model Combustor Calculated with k-Epsilon Model," *International Journal of Thermal Sciences*, Vol. 43, No. 9, 2004, pp. 901–914.

[19] Wang, P., and Bai, X. S., "Large Eddy Simulations of Turbulent Swirling Flows in a Dump Combustor: A Sensitivity Study," *International Journal for Numerical Methods in Fluids*, Vol. 47, No. 2, 2005, pp. 99–120.
[20] Wang, P., Bai, X. S., Wessman, M., and Klingmann, J., "Large Eddy Simulation and Experimental Studies of a Confined Turbulent Swirling Flow," *Physics of Fluids*, Vol. 16, No. 9, 2004, pp. 3306–3324.
[21] Derksen, J. J., "Simulations of Confined Turbulent Vortex Flow," *Computers and Fluids*, Vol. 34, No. 3, 2005, pp. 301–318.
[22] Grinstein, F. F., Young, T. R., Gutmark, E. J., Li, G., Hsiao, G., and Mongia, H. C., "Flow Dynamics in a Swirl Combustor," *Journal of Turbulence*, Vol. 3, No. 30, 2002.
[23] Guo, B., Langrish, T. A. G., and Fletcher, D. F., "CFD Simulation of Precession in Sudden Pipe Expansion Flows with Low Inlet Swirl," *Applied Mathematical Modelling*, Vol. 26, No. 1, 2002, pp. 1–15.
[24] Melling, A., "Tracer Particles and Seeding for Particle Image Velocimetry," *Measurement Science and Technology*, Vol. 8, No. 12, 1997, pp. 1406–1416.
[25] *PivView2C, User Manual, Ver. 2.1*, PIVTec GMBH, Germany.
[26] Beer, J. M., and Chigier, N. A., *Combustion Aerodynamics*, Applied Science Publishers, Ltd., London, U.K., 1972, Chap. 5.
[27] Panduranga Reddy, A., "A Study of Swirler Flow Field Characteristics in a Sudden Expansion Square Chamber Using PIV," Masters Thesis, Department of Aerospace Engineering, IIT Madras, India, 2004.
[28] Schram, C. F., "Aeroacoustics of Subsonic Jets: Prediction of the Sound Produced by Vortex Pairing Based on Particle Image Velocimetry," Ph. D. Dissertation, Physics Department, Technical University Eindhoven, The Netherlands, 2003.
[29] Tunnekes, H., and Lumley, J. L., *A First Course in Turbulence*, MIT Press, Cambridge, 1972.
[30] Schram, C. F., Rambaud, P., and Riethmuller, M. L., "Wavelet Based Eddy Structure Eduction from a Backward Facing Step Flow Investigated Using Particle Image Velocimetry," *Experiments in Fluids*, Vol. 36, No. 2, 2004, pp. 233–245.

A. Gupta
Associate Editor